이학박사 학위논문

A Lipid-Nanopillar-Array-Based Immunosorbent Assay for Virus Detection

지질 이중층 나노필라 어레이 기반 면역 흡착법을 통한 바이러스 검지

2021 년 2 월

서울대학교 대학원
화학부 무기화학

김 지 은

A Lipid-Nanopillar-Array-Based
Immunosorbent Assay for Virus Detection

지질 이중층 나노필라 어레이 기반
면역 흡착법을 통한 바이러스 검지

지도교수 남좌민

이 논문을 김지은 박사 학위논문으로 제출함
2021 년 1 월

서울대학교 대학원
화학부 무기화학
김지은

김지은의 박사 학위논문을 인준함
2021 년 1 월

위 원 장 이현우 (인)
부 위 원 장 남좌민 (인)
위 원 민달희 (인)
위 원 송윤주 (인)
위 원 이진석 (인)

Abstract

A-Lipid-Nanopillar-Array-Based Immunosorbent Assay for Virus Detection

Jieun Kim

Department of Chemistry, Inorganic Chemistry

The Graduate School

Seoul National University

Since infectious diseases, particularly viral infections, have threatened human health and caused huge economical losses globally, a rapid, sensitive, and selective virus detection platform is highly demanded. Enzyme-linked immunosorbent assay (ELISA) with flat solid substrates has been dominantly used in detecting whole viruses for its straightforwardness and simplicity in assay protocols, but it often suffers from limited sensitivity, poor quantification range, and a time-consuming assay procedure.

Here, a lipid-nanopillar-array-based immunosorbent assay (LNAIA) is developed with a nanopillar-supported lipid bilayer substrate with fluorophore-modified antibodies for rapid, sensitive, and quantitative detection of viruses. 3D-nanopillar array structures and fluid antibodies with fluorophores facilitate faster and efficient target binding and rapid fluorophore localization for quick, reliable

analysis on binding events with a conventional fluorescence microscopy setup. LNAIA enables quantification of the H1N1 virus that targets down to 150 virus particles with the 5-orders-of-magnitude dynamic range within 25 min, which cannot be achieved with conventional ELISA platforms.

Keywords: biosensors, immunosorbent assays, lipid nanopillar arrays, supported lipid bilayers, virus detection

Student Number: 2014-21220

Contents

Citation to Previously Published Work

Chapter 2 have appeared in or modified from the following paper and its supplementary online material:

"A Lipid-Nanopillar-Array-Based Immunosorbent Assay", Jieun Kim, Sungi Kim, Junhyoung Ahn, JaeJong Lee, Jwa-Min Nam, *Advanced Materials*, 2001360, (2020)

Chapter 1. Introduction

1.1. Virus assay methods

Enzyme-linked immunosorbent Assay (ELISA) is used as a "gold standard" for whole virus detection.[1–3] The step of intrinsic signal amplification using enzyme labels produces thousands of optically measurable signals and facilitates quantitative measurement of viruses. Despite the advantages of ELISA, selectivity is limited according to the quality of antibodies and several washing steps and amplification steps limit the throughput of ELISA. To avoid the shortcomings induced by antibodies, aptamer, molecular imprint polymers (MIP),[4–7] camelid antibodies,[8,9] and monoclonal antibodies were developed.

To detect viruses, targets must be converted to visible readout via labels such as fluorescent molecules. The fluorescence immunoassay (FIA) can detect the analyte without amplification phase, but the background signal reduces the sensitivity of the test.[10] Thus, sophisticated microscopic settings, such as total internal reflection fluorescence microscopy (TIRFm) and time-resolved fluorescence immunoassay (TRF), were developed to compensate for the shortcomings of non-evaporation fluorescence-based testing.[11] Despite the above-mentioned virus detection methods have each advantage, sophisticated set-up of equipment impedes accessibility and lower throughput of the assay.

1.2. Supported lipid bilayers and nanostructure

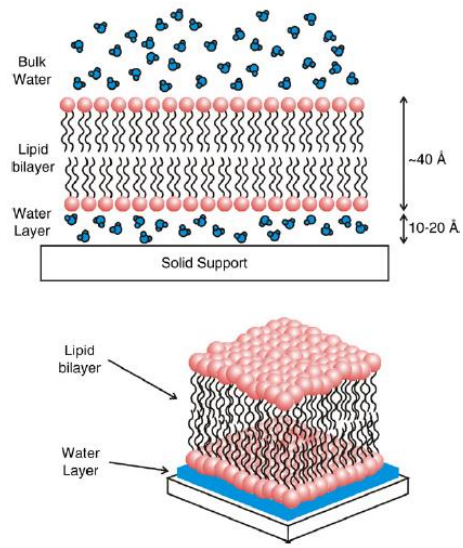

Figure 1-1. Schematic diagram of a solid supported phospholipid bilayer. The membrane is separated from the substrate by a 10−20 ˚A thick layer of water.

The lipid bilayer is one of the most eloquent and important self-assembled structures in nature. It not only provides a protective container for cells and sub-cellular compartments, but also hosts much of the machinery for cellular communication and transport across the cell membrane. Solid supported lipid bilayers (SLBs) provide an excellent model system for studying the surface chemistry of the cell.[12,13] Moreover, they are accessible to a wide variety of surface-specific analytical techniques.[14,15] This makes it possible to investigate processes such as cell signaling, ligand–receptor interactions, enzymatic reactions

occurring at the cell surface, as well as pathogen attack. Supported lipid bilayers (SLBs) provide cell membrane-like environments for studying various surface-based technology[16]. Owing to these properties, SLBs have been used as model systems for biological cell membrane. For example, the two-dimensional large fluidity allows the dynamic movement of biomolecules on SLB and investigation

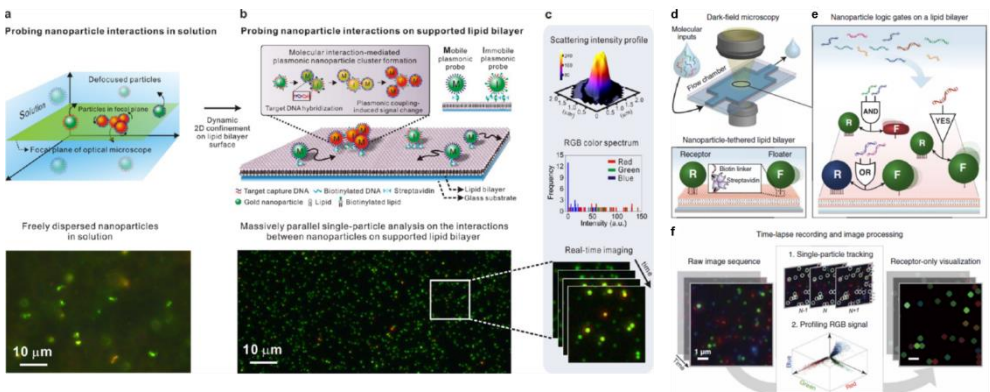

Figure 1-2. Plasmonic nanoparticle dynamically tethered on SLB for single-nanoparticle-level in situ parallel imaging and analysis. a) Freely dispersed nanoparticles in three-dimensional motion (top). Dark-field microscopy image of 50-nm gold nanosphere in solution (bottom). b) Dynamic two-dimensional confinement of plasmonic nanoparticles on lipid bilayer surface (top). In situ observation and analysis o SLB-tethered plasmonic nanoprobes via dark-field microscopy with single particle resolution. c) Quantitative analysis of single plasmonic cluster. d) Single-nanoparticle level observation on SLB for logic computation. e) Schematic illustration of logic operation with RGB plasmonic nanoparticles. f) Single particle tracking algorithm.

of biological process at the cellular level, providing ligand-receptor interactions, viral attack, enzymatic reactions, and cellular signaling.[1,17–22] Moreover, by tethering plasmonic nanoparticles on SLB, it is possible to study and manipulate interactions between nanoparticle in single-particle resolution (**Figure 1-2**).[23–25]

SLBs have been blended with a nanostructured substrate for a wide range of applications. In the initial stage of SLB-nanostructure hybridization, Jay T. Groves and coworkers used an inert barrier to vesicle fusion for creating patterned SLB (**Figure 1-3**).[26,27] SLB was formed on a silicon oxide substrate and partitioned by a photoresist barrier.

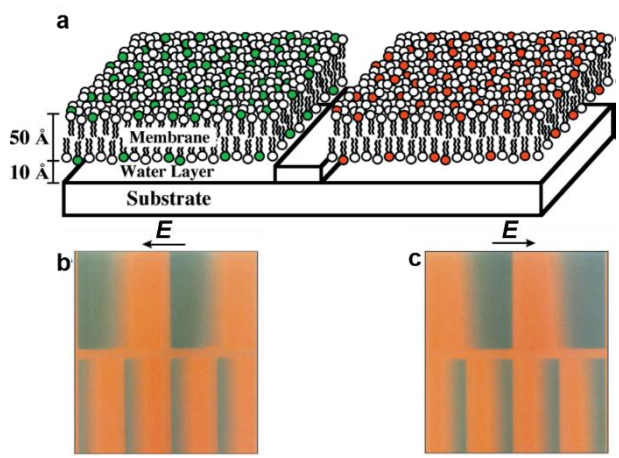

Figure 1-3. a) Schematic diagram of a supported lipid bilayer partitioned by a microfabricated photoresist barrier. b,c) Epifluorescence image of electric field (*E*)-induced concentration gradients of negatively charged fluorescent lipid (TexasRed-DHPE) in membranes confined by microfabricated corrals. (b) and (c) are 400 μm × 400 μm.

Due to SLB uniformly distribute on a hydrophilic substrate such as glass, quartz, silicon wafers, and polydimethylsiloxane (PDMS), hydrophobic materials are used as a barrier of SLB. Kei Murakosh and coworkers used gold as a nanoratchet to study the effect of Brownian motion of freely diffusing lipid molecule[28]. Kam and others also studied directional movements of lipid molecules with ordered nanoratchet made of photoresist and nanogrooves (**Figure 1-4**).[28–30]

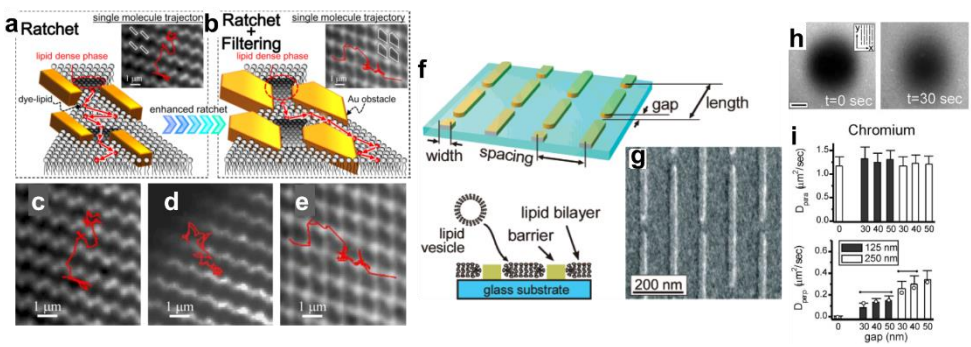

Figure 1-4. Brownian ratchet for SLB with various size and shape. a, b) Size and shape of ratchet obstacles manipulate Brownian motion of lipid molecules of SLB. c, d, e) Typical trajectories of bright objects observed while spreading a lipid bilayer on a ratchet substrate with three different ratchet obstacles. f) Schematic illustration of chromium nanobarrier for non-Brownian diffusion of lipid molecules. g) SEM image of nanobarrier array. h) Anomalous diffusion of TexasRed-DHPE lipids of nanobarrier array. i) Mean square displacement of lipid with parallel direction (D_{para}) and perpendicular direction (D_{perp}) to nanobarrier.

Black lipid membranes consist of phospholipid molecules painted across a hole between two solution chambers (**Figure 1-5**). Black lipid membranes are suspended in solution and there are no interferences of the membrane with underlying support. By controlling the structure and material of nanostructured mechanical support and composition of lipids, suspended SLB without interfaces of the membrane with underlying support can be generated. The absence of such support also means that transmembrane proteins suspended within the phospholipid bilayer remain fully mobile and active. A porous membrane with pore diameter ranging from ~10 to ~100 nm with anodic aluminum oxide, polycarbonate membranes, and photolithographically generated silicon membranes was applied to form black lipid membranes.[31–34] However, this also limits the lifetime of the bilayer due to the poor stability of the membrane. The detection method employed with black lipid membranes is also typically limited.[35]

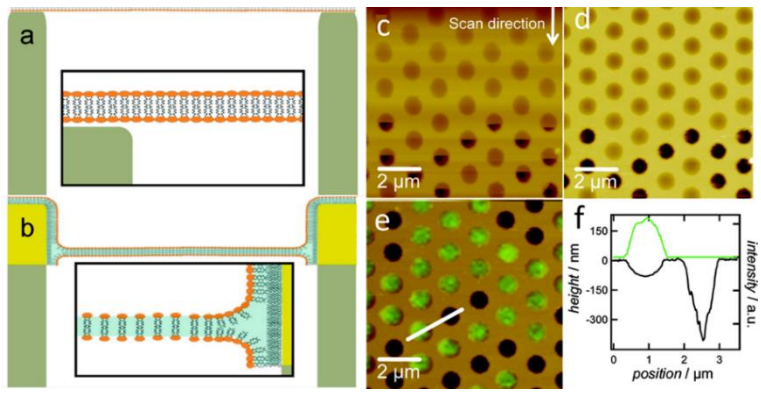

Figure 1-5. Suspended lipid membrane on nanostructure. a) Schematic representation of solvent-free supported bilayers prepared on hydrophilic porous silicon substrates exhibiting negligible prestress. The bilayer on the pore rims can easily slide into the pore upon indentation. The response is bending and tension dominated. b) Illustration of a hybrid pore-spanning membrane showing substantial prestress. A gold layer of 60 nm on top of the silicon substrate was equipped with a self-assembly layer of octanethiol prior to membrane deposition either via painting of lipids or spreading of giant liposomes. c) Topographic AFM image (contact mode) obtained at a loading force of 300 pN showing rupture events during the first AFM scan. d) Second scan also at a loading force of 300 pN displaying the pattern of open pores occurred after the first scan. e) Overlay of fluorescence (green) and AFM topography (brown) images of DPhPC/BodipyPC (99:1)/OT nano-BLMs on a porous silicon substrate with a pore radius of 400 nm. f) Height and fluorescence profiles (along white line in (e)) of a membrane-covered and uncovered pore.

1.3. Nanostructured SLB for biodetection

Cui group approved highly selective capture efficiency of circulating tumor cells on 5-nm gap lipid nanopillar array by preventing nonspecific binding and boosting capture efficiency, presenting antibody uniformly, and allowing antibody clustering upon cell capture to strengthen the cell-surface interaction. This nanostructured lipid bilayer fulfills the needs of CTC cell study on high capture efficiency and high capture purity (**Figure 1-5**).[36] Metal@silica nanoparticle in solution was also hybridized with SLB for measuring protein-SLB membrane interaction through localized-surface plasmon resonance (LSPR) shift by Jay. T. Goves group in 2012.[37]

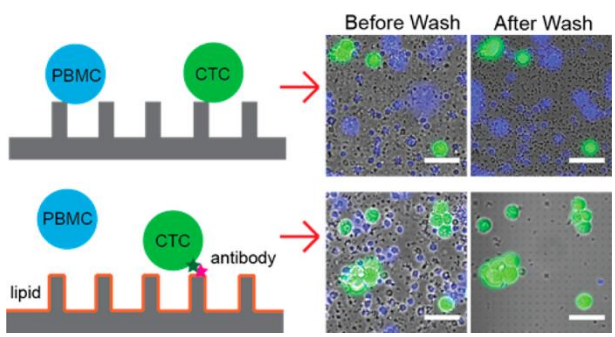

Figure 1-6. Circulating tumor cell (CTC) detection by boosting capture efficiency and capture purity using nanostructured surface and SLB.

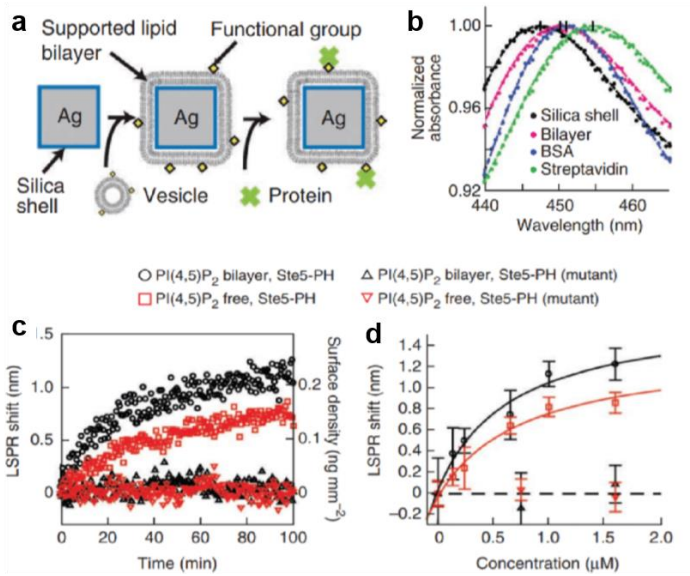

Figure 1-7. Schematic illustration of a SLB coated Ag@SiO_2 nanocube assay (a) and LSPR shift of nanocubes upon sequential addition of lipid vesicle, bovine serum albumin (BSA), and streptavidin (b). Nanocube-based time-dependent binding kinetics (c) and equilibrium binding curves (d) of wildtype and mutant Gst-Ste5 pleckstrin homology to lipid membrane with and without L-α-phosphatidylinositol-4,5-bisphosphate (PI(4,5)P2).

Nam group developed electrofluidic lipid membrane biosensing platform with patterned and partitioned SLB for detection of cholera toxin B (CTB) (**Figure 1-7**).[38] When electric field applied to the electrofluidic lipid membrane applied,

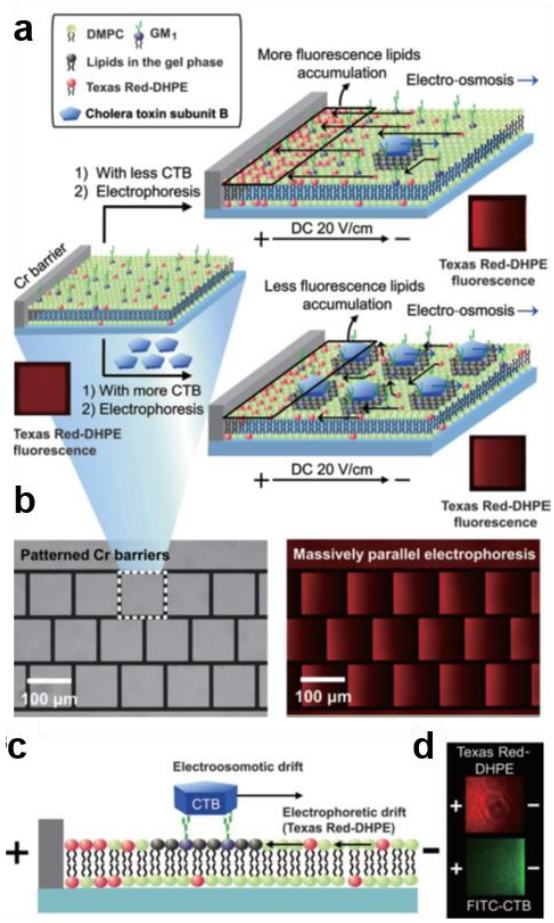

Figure 1-8. a) Schematic illustration of the electrofluidic lipid membrane biosensor. Red insets are epifluorescence microscope images of the SLB and each corresponds to the adjacent diagram. b) Left: Optical microscope image of multiple Cr corrals patterned on a glass substrate. Right: Parallel and simultaneous electrophoresis of multiple SLB patterns.

depends on the target concentration, negatively charged, fluorophore-labeled lipids, i.e., in this case (Texas Red)–1,2-dihexadecanoyl-sn-glycero-3-phosphoethanolamine (Texas Red–DHPE) moves toward a positive electrode. The target concentration was quantified through fluorescence microscopy analyzing the flow of FITC-CTB and the flow of DHPE.

Recently, Huskens group developed SLB-based multivalent recombinant hemagglutinin(rHA) detection platform via quartz crystal microbalance with dissipation monitoring (QCM-D) measurement. Hemagglutinin, a protein on the influenza virus specifically binds to sialic acid (SA)-terminated carbohydrates present at the cell membrane. SLB containing sialyl lactosamine mimics the cell membrane and rHA nanoparticles used as an mimic of influenza virus to provide prediction of the number of interactions involved in virus-cell binding.[39]

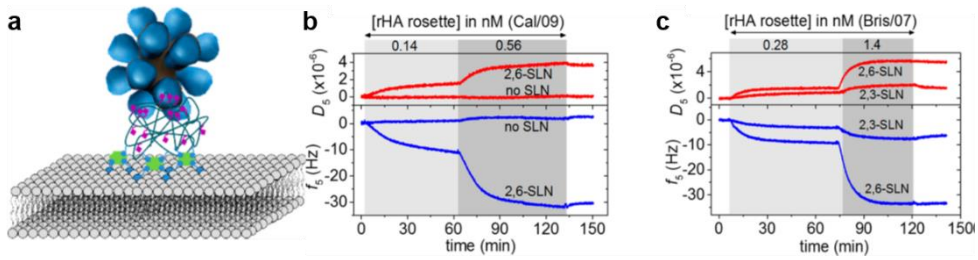

Figure 1-9. a) Schematic illustration of the SLN-modified SLB platform and its interaction with rHA nanoparticles. b,c) Selectivity of the binding of rHA rosettes at the SLB platform b) QCM-D results of the binding of A/California/07/2009 (Cal/09) rHA rosettes to SLBs modified with biotin-PAAm-2,6-SLN or biotin-PAAm (without SLN). c) QCM-D results of the binding of A/Brisbane/59/07 (Bris/07) rHA rosettes to SLBs modified with biotin-PAAm-2,6-SLN or biotin-PAAm-2,3-SLN. PAAm: poly[N-(2- hydroxyethyl)acrylamide], SLN: sialyl lactosamine

Chapter 2. A lipid-nanopillar-array-based Immunosorbent Assay for Virus Detection

2.1. Research background

Since viruses manipulate and inhibit the host immune system, viral pandemics, such as COVID-19, African swine fever, Ebola, and influenza, threaten the lives of humans and livestock.[2,40,41] Viral pandemics are mainly induced by silent spread from untreated hosts with undiagnosed infections. To treat the infected individuals in a timely, precise manner and prevent serious epidemics, rapid, sensitive, and selective virus detection using a straightforward method is required.[42] Widely used virus detection methods are based on polymerase chain reaction (PCR) that amplifies target genes, ELISA, and rapid influenza diagnostic test (RIDT) that detect the whole virus. Although the whole virus detection methods are straightforward and do not require further sample processing, they are time-consuming and labor-intensive. Conventional chip-based biosensors for virus detection, such as ELISA, immobilize the capturing molecules (e.g., antibodies) on a solid substrate for target detection, and require laborious downstream labeling which transforms the concentration of the captured target into an optical signal.[2,41] Although widely adopted given the simplicity of the method, ELISA does not offer high sensitivity, high specificity, and reliable quantification for viral targets within a short period. This means that, although requiring target sequence to generate the

primers for selective target amplification, prone to errors due to DNA polymerase, susceptible to nonspecific binding of the primers to other similar sequences on the template DNA and requiring complex setup for temperature-dependent cycles and signal measurements, PCR is the only highly reliable method in precise and accurate detection of viruses.

2.2. Results and discussion

Supported lipid bilayer (SLB), synthetic fluid lipid bilayer on a solid substrate, hybridized with nanostructures has been utilized for various biotechnological applications because of the dynamic movement of the lipids similar to cell membrane while skimming complex proteins and substantial experimental uncertainty.[12,15,43–45] Moreover, SLB provides a reaction platform with a two-dimensional focal plane for imaging and analysis of interactions between plasmonic nanoparticles tethered to SLB at a single-particle level.[23,46] Here, we developed an immunosorbent whole virus assay on a nanofabricated SLB, termed a lipid nanopillar array-based immunosorbent assay (LNAIA), inspired by the dynamic movement and clustering of receptors on a host cell membrane when a virus is engulfed into the cell through endocytosis (**Figure 2-1**).[47,48] The biotinylated antibodies with Cy3 fluorescent dyes (Cy3-antibodies) tethered onto a lipid nanopillar array (LNA) by streptavidin linkers can dynamically move along on an LNA (**Figure 2-1**. b-c). In LNAIA, when target viruses are introduced to the

LNA, they are captured by the freely diffusing Cy3-antibodies and eventually surrounded by multiple Cy3-antibodies on the bottom surface and the sidewall of the pillars that generate three-dimensional polyvalent interactions with the antibodies (**Figure 2-1**. d-f). They create localized and immobilized fluorescent spots that are clearly distinguishable from the fluorescent background with a routinely used epifluorescence microscope. Because the number of hemagglutinin (HA) molecules on the viral surface is greater than neuraminidase (NA) by an order of magnitude,[49] a strong fluorescent signal can be obtained by the efficient localization of multiple HA-specific, Cy3-antibodies.

2.2.1. Basic setups of lipid-nanopillar-array based immunosorbent assay for virus detection

The nanopillar array underlying SLB was engineered to form nanostructural protrusions, enhancing rapidity and sensitivity of the target virus detection by providing a larger surface area and the 3D labyrinth-like environment with the dynamic movement of fluorescent antibodies that facilitate the target viruses to abundantly collide with the tethered Cy3-labelled antibodies. The silica nanopillar array fabricated by resist-free direct UV/thermal nanoimprint lithography provides sufficient hydrophilicity for stably forming SLB on the substrate. The nanopillar array is 200 nm in diameter and height and has 200 nm gaps between pillars, creating a hexagonal array (**Figure 2-1**. a, j and **Figure 2-2**)

so that maximizes the collisions between viruses and the nanopillars and enables the fast, efficient capture of an 80-120 nm-sized influenza virus with multiple antibodies by three-dimensional polyvalent antigen-antibody interactions.

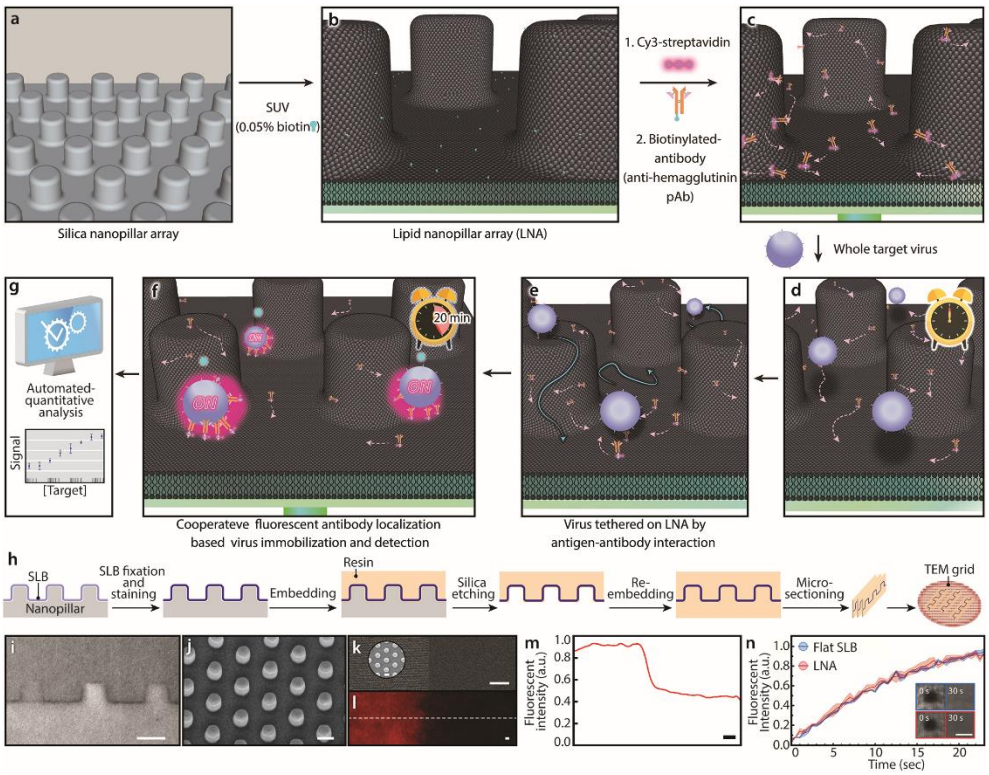

Figure 2-1. Lipid-nanopillar-array-based immunosorbent assay (LNAIA) for rapid, sensitive virus detection. a–g) Schematic of LNAIA. h) Experimental procedure of transmission electron microscopy (120 kV, Talos L120C, FEI, Hillsboro, United States) of the lipid bilayer formed on the nanopillar-patterned substrate. i) TEM image of the microsectioned LNA. j) SEM image of a tilted nanopillar substrate. k) SEM image of the pillar-to-flat boundary area. l) fluorescence microscopic image of 1% Texas Red-modified SLB formed on the pillar-to-flat boundary area. m) Fluorescence intensity line profile on the dotted line of (e). n) Fluorescence recovery after photobleaching (FRAP) results of the nanopillar patterned substrate and a flat substrate (inset). Diffusion coefficients of flat SLB and nanopillar SLB are ≈ 0.34 and ≈ 0.35 μm^2 s^{-1}, respectively. The colored areas in the plots represent mean standard errors. The scale bars in (i, j) and (k–n) are 200 nm and 5 μm, respectively.

In a typical experiment, LNAIA requires ~25-min assay time after loading

analytes, and the stepwise assay procedure is shown in **Figure 2-1**, **Figure 2-9**, and the Experimental Section. In the attached 8-μL silicon chamber on a hydrophilic silica nanopillar array, small unilamellar vesicles (SUV) with 0.05% biotinylated-DOPE in 150 mM PBS was introduced. The ruptured vesicles in the chamber then form a lipid bilayer on a supporting nanopillar array. After washing excess SUVs, Cy3-labeled streptavidin and biotinylated polyclonal HA-specific antibody were introduced to the chamber. A ratio of biotinylated-DOPE in liposome affects the surface density of Cy3-labeled antibodies on LNA and can eventually affect the fluorescence signal to background ratio during the assay. We optimized the biotinylated-DOPE ratio and added amounts of streptavidin and antibody to maximize the detection sensitivity while minimizing assay time and nonspecific bindings. Before loading analytes, we imaged the substrate with a conventional fluorescence microscope. 20 min after loading 8 μL of analytes, we imaged and quantified the number of newly formed fluorescent spots (ΔN) in the chamber with an automated ImageJ software.

We first characterized the formation of SLB on the nanopillar array by transmission electron microscopy (TEM) (120 kV, Talos L120C, FEI, Hillsboro, United States) and fluorescence microscopy (TE-2000, Nikon, Tokyo, Japan) (**Figure 2-1**. h-n, **Figure 2-2**. c). SLB was designed to fully cover the sidewall and top part of the nanopillars and the bottom of the substrate for efficient virus capture between the pillar wall and the bottom surface. For characterization of the SLB

coverage on a nanopillar substrate, the phosphate head groups of SLB were dyed by uranyl acetate, embedded in Spurr's resin, micro-sectioned via ultramicrotome, and observed via TEM (**Figure 2-1**. h, i and **Figure 2-2**). The dark line in **Figure 2-1**. i and **Figure 2-2**. c reveals that the dyed SLB closely follows the nanopillar substrate surface.

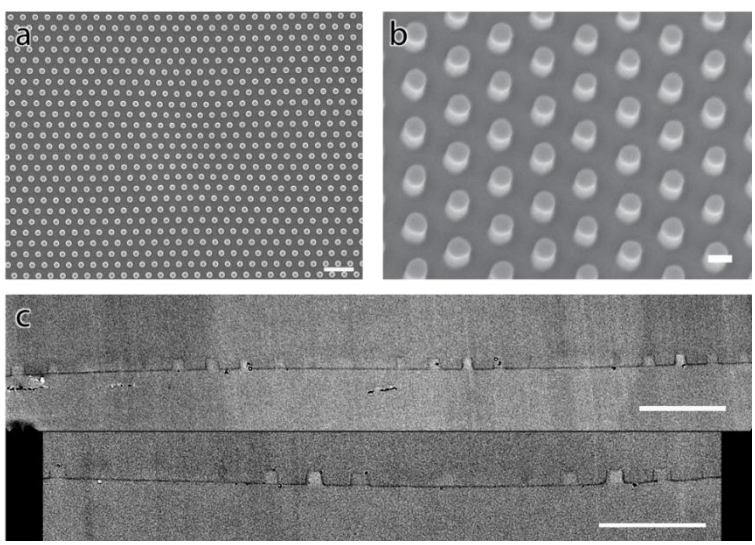

Figure 2-2. Electron microscopy images of a nanopillar array and lipid nanopillar array. a) A large-scale SEM image of a nanopillar pattern. b) A tilted SEM image of a nanopillar substrate. c) TEM images of sectioned LNA. Scale bars in (a, c) and (b) are 1 μm and 200 nm, respectively.

Due to the high surface area of the nanopatterned array as compared to a flat substrate, the fluorescence intensity of the nanopatterned substrate was much stronger than is seen on a flat surface. We calculated the theoretical surface area ratio between the pillar-patterned and flat areas for comparison with the fluorescence intensity ratio (**Figure 2-1**. k-m).

$A_{cell}/A=1+2hp/R=2.05$ (**Equation 1**)

A_{cell} is the total surface area of a unit cell containing a single cylindrical pillar, A is the surface area of a unit cell without a pillar, *h* is the height of a pillar (200 nm), p is the surface coverage of the pillars, and R is the radius of a pillar (100 nm). This calculation yielded a ratio of 2.05, which closely matched the measured fluorescence ratio of 1.93, further indicating SLB formation along with the nanopillar pattern (**Figure 2-1**. k- m).

We conducted fluorescence recovery after photobleaching (FRAP) experiments to investigate the fluidity of the SLB on a nanopillar substrate (**Figure 2-1**. n). The degree of fluorescence recovery after bleaching indicates that SLB covers the nanopillar substrate without losing fluidity. In previous studies combining nanopatterned substrates and SLB, SLB either did not fully cover the nanopattern or formed a suspended structure due to either hydrophobic surface[28] or unsuitable liposome size.[35] In LNAIA, the nanopillar substrate was made of

silica to achieve high hydrophilicity and proper dimensions, enabling the homogeneous formation of a lipid bilayer along with the nanopillar on the substrate. We then monitored localization events of fluid and fluorescent antibodies around the target virus via conventional epifluorescence microscopy. After preparing the LNAIA kit as described in the Experimental Section, we captured fluorescent images before and after a 20-minute sample loading. As an H1N1 virion approaches the antibody modified LNA, multiple polyclonal antibodies bind to the virus, localizing the fluorescent antibodies to an area roughly the size of a single virus. The concentrated antibodies generate a readily detectable fluorescent spot corresponding to a single virus with a high signal to background noise ratio.

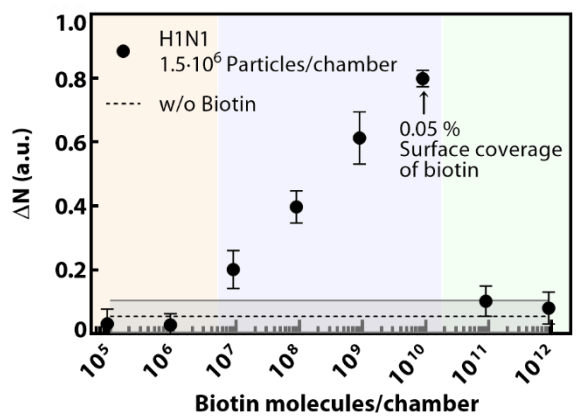

Figure 2-3. Correlation between efficiency of fluorescence spot generation and biotin coverage on LNAIA. The dotted line is LNAIA result without biotin.

A correlation between coverage of antibody on LNAIA and the number of fluorescence spots was studied (**Figure 2-3**). On LNAIA, the surface coverage of

the antibody has a linear correlation with the biotin ratio in a lipid bilayer. Controlling the biotin ratio in the lipid bilayer, the number of newly formed fluorescent spots (ΔN) were counted with $1.5X10^6$ H1N1 particles/chamber in 150 mM phosphate-buffered saline. In the two cases, fluorescent spots were not formed after assay. First, when the number of biotins is relatively insufficient toward the number of virus in a chamber, Cy3-antibody was not localized, and no fluorescent spot was formed (Yellow area in **figure 2-3**). Second, in the case of the greater number of biotins, the high surface density of Cy3-antibody makes high background noise and hinders localization of them for generating fluorescent spots having a high signal-to-noise ratio (Green area in **Figure 2-3**).

2.2.2. Virus capture and mobility studies on a lipid nanopillar array

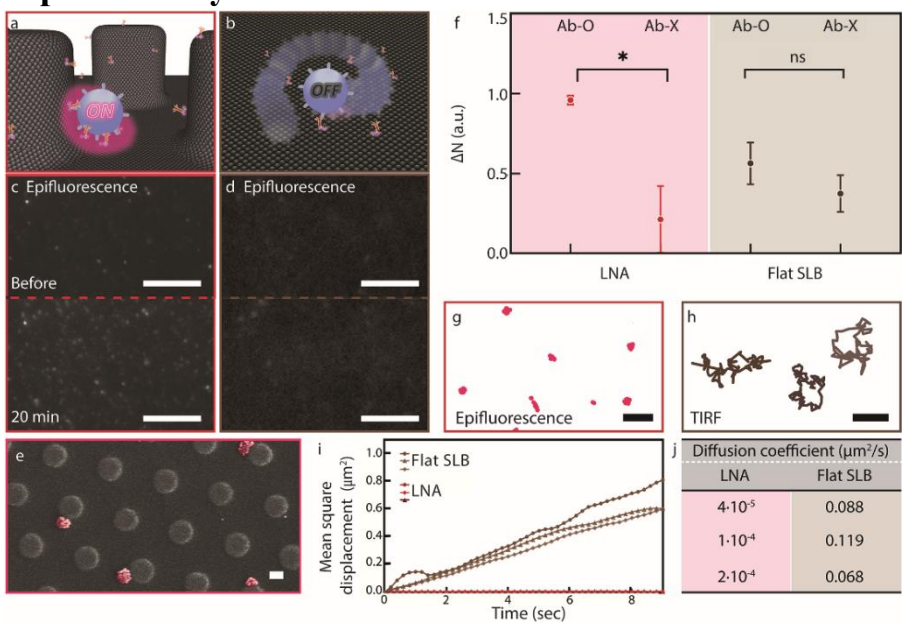

Figure 2-4. Virus capture and mobility studies on nanopillar and flat SLB substrate. a) Illustration of a trapped virus on the nanopillar SLB after assay. b) A freely moving virus on a flat SLB after assay. Epifluorescence microscopy images on c) lipid nanopillar array (LNA) and d) flat SLB before and after assay. e) SEM image of substrate after assay. The SEM image was acquired after freeze-drying. f) LNAIA results on each SLB with antibody (Ab-O) and without antibody (Ab-X). The p-value between Ab-O and AB-X on the LNA was 0.0286. *$p < 0.05$ (one-tailed Mann–Whitney U test). Trajectory of fluorescence spots g) on the nanopillar SLB via an epifluorescence microscope and h) flat SLB via TIRF microscope. i) Mean square diameter and j) diffusion coefficient of fluorescence spots on each SLB after assay. The scale bars in (c, d), (e), and (g, h) are 5 μm, 100 nm, and 1

For quantitative virus detection, we automatically counted ΔN with >1.5 of the signal-to-noise ratio using a particle-counting software (MosaicSuite particle tracker plugin of image J). We found that the nanopillar array structure plays an important role in increasing assay sensitivity and target capturing efficiency. The fast, strong colocalization of Cy3-antibody and immobilization of target virus resulting from the three-dimensional antigen-antibody interactions generate a high fluorescence signal to background signal ratio that enables efficient target detection by conventional fluorescence microscopy. The position of virus on LNA is typically between the sidewall of a pillar and the bottom surface, as seen in an SEM image of the freeze-dried substrate, after assay, further showing the importance of protruding nanopillar structures with a hexagonal array for efficient capture of viruses (**Figure 2-4**. e, **Figure 2-5**) The ΔN value with the LNA was significantly larger than the control experiment case without antibody obtaining the p-value of 0.0286, while the flat SLB generated a similar ΔN value to the control experiment result having the p-value of 0.028 (**Figure 2-4**. f)

To detect a single fluorescent spot by fluorescence microscopy, minimal distance to identify two individual entity which is dependent on the numerical aperture of a microscope objective lens, an emission wavelength of a fluorophore, and pixel and number of CCD must be considered. Considering the numerical aperture of the objective lens (1.49) and an emission wavelength of dye (570 nm) in our experimental setup, the resolution of the epifluorescence microscopy is

about 190 nm. A fluorescent spot is visible when fluorophores within a diffraction limit emit the number of photons twice over the noise signal from the background. Comparing the number of antibodies that connect the virus to flat SLB and LNA, a lower number of antibodies binds to SLB. On LNA, fluorescence spots with a high signal-to-noise ratio are observable via epifluorescence microscopy from highly localized Cy3-antibody surrounding a virus. (**Figure 2-4**. g)

Furthermore, as mentioned above, because viruses are immobilized between the sidewall and the bottom surface with multiple antibodies, the signal-to-noise ratio of the fluorescence spots gets higher with long exposure time. (**Figure 2-4**. g) On the other hand, on flat SLB, because of the lower number of antibodies per virus and dynamic movement of the virus along with SLB, the signal-to-noise ratio does not increase with long exposure time via epifluorescence microscopy. Trajectories in **Figure 2-4**. h indicate freely diffusing viruses tethered with a smaller number of antibodies on flat SLB imaged via TIRF, and they are not observable via epifluorescence microscopy. It should also be noted that LNA boosts the binding kinetics of the virus to the surface antibodies due to the enlarged surface area and multiple protrusions enhancing the collisions between surface and virus.

A distance between the nanopillars of the hexagonal array affected the sensitivity of LNAIA. The number of pillars decreases as the distance between

pillars increases. A fluorescence spot with noticeable signal-to-noise ratio forms when a target virus is fixed between the sidewall of a pillar and the bottom surface by localized fluorescence-antibody. The longer the distance between nanopillars, the lower the number of nanopillars per unit area, the lower the surface area, the lower the chance of viruses being fixed, and finally the less sensitivity of the assay.

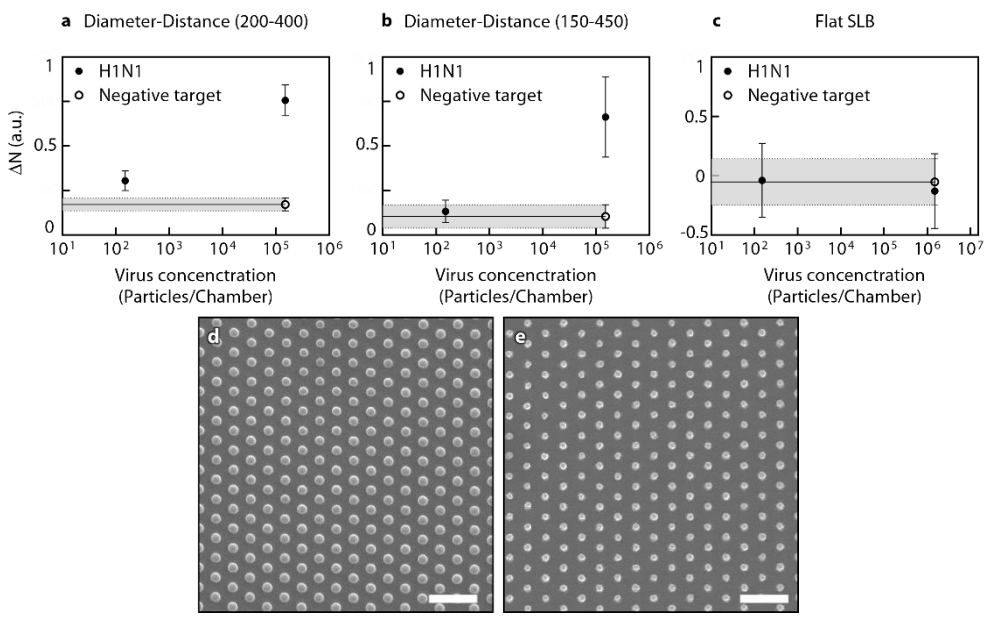

Figure 2-5. Assay sensitivity depending on the distance between nanopillars in a hexagonal nanopillar array (a-c). SEM images of nanopillar arrays with 200 nm diameter and 400 nm distance (d), and 150 nm diameter and 450 nm distance (e). Scale bars are 1μm.

2.2.3. LANIA results for H1N1 virus detection

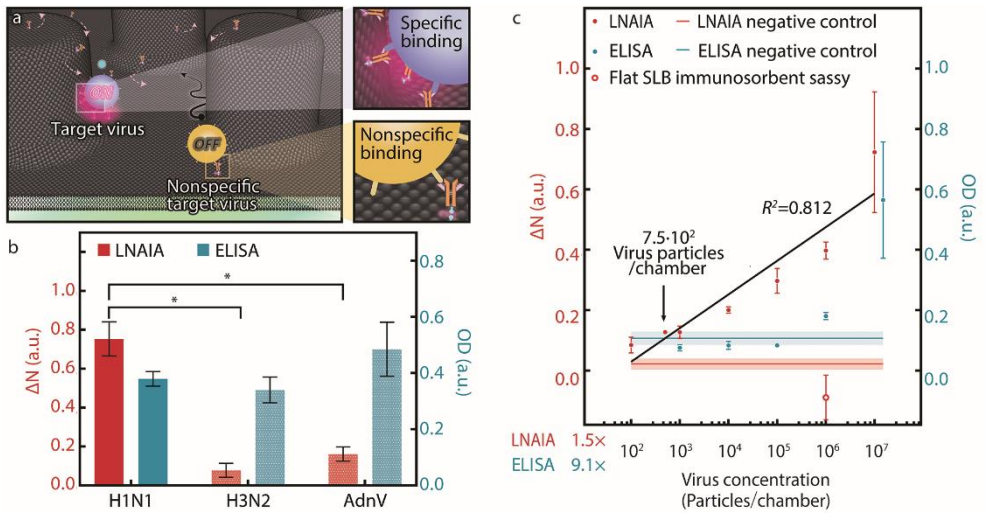

Figure 2-6. LNAIA results for H1N1 virus detection. **a)** Elimination of false-positive results by weak fluorescence-signal-based paucivalent nonspecific bindings. The weak nonspecific binding between the fluorescent antibody and the nontarget virus induces a very low number of virus-captured fluorescent dyes, and this creates a weak fluorescent spot with a low signal-to-noise ratio. **b)** LNAIA and ELISA results for H1N1 target and nontarget viruses (1.5×10^5 particles per chamber for LNAIA and 9.1×10^5 particles per chamber for ELISA). In LNAIA, the p-value for H1N1 compared to H3N2 and AdnV was 0.028. *$p < 0.05$ (one-tailed Mann–Whitney U test). c) Quantitative analysis of H1N1 virus detection in human serum using LNAIA and ELISA. After virus loading, ELISA required roughly 6 h while LNAIA required 25 min, including data analysis. Negative control was conducted with 1.5×10^5 and 9.1×10^5 particles per chamber of adeno virus for LNAIA and ELISA, respectively. The plotted data represent mean ± standard deviation.

Furthermore, nonspecific viruses, H3N2, and adenovirus (AdnV) were not differentiated from the target virus at low concentration with ELISA (**Figure 2-6**. b). Although we used the same antibody for both LNAIA and ELISA, LNAIA showed significantly higher selectivity compared to ELISA (**Figure 2-6**. b). We attribute this selectivity to the following hallmarks of LNAIA. Signal generation is accomplished by the cooperative interaction between the Cy3-antibody and the viral target. False-positive signals are efficiently eliminated with LNAIA because true positive signals are only produced when the concentration of Cy3-antibody exceeds the threshold of the fluorescence microscope, and each individual clustered spots can be reliably imaged and analyzed only when virus targets were multivalently captured by fluorescent antibodies (**Figure 2-6**. a). Besides, extracellular molecules in analytes cannot be bound by SLB, an artificial cell membrane without membrane proteins – SLB is an excellent surface with minimal nonspecific bindings. This is further supported by lower background signals with the LNAIA negative control than with the ELISA-based negative control (**Figure 2-6**. c).

Importantly, the mean of ΔN values with LNAIA display a linear relationship through at least 5 orders of magnitude of target quantity. The limit of detection of LNAIA is about 150 virus particles, which showed 4 orders of magnitude higher sensitivity than commercially available H1N1 ELISA. Moreover, LNAIA requires only 25 minutes while ELISA required >3 hours due

to laborious antigen binding, labeling, and washing procedures (**Figure 2-6**. c, **Figure 2-7**). LNAIA can be much faster than other conventional assays such as ELISA because the fluorescent antibodies on LNA are highly mobile, allowing more active and cooperative interactions with virus targets, nanopillar structures induce more efficient and faster binding between fluid antibodies and viruses, and lipid bilayer surface is an excellent substrate with minimal nonspecific bindings.

Furthermore, due to a signal generation mechanism, LNAIA significantly surpasses the selectivity of ELSIA. Even though a dissociation constant of antibody towards a target virus is much lower than towards a nonspecific virus, binding of the nonspecific virus to antibody can be transduced into an optical signal and contributes to an ensemble signal in ELISA. On the other hand, in LNAIA, the number of antibodies per target virus particle is much higher than per nonspecific virus particle. Because localized dye molecules in diffraction limit generate a fluorescence spot, the spot is not generated from the nonspecific virus particle. Therefore, the selectivity of LNAIA is higher than ELISA (**Figure 2-7**).

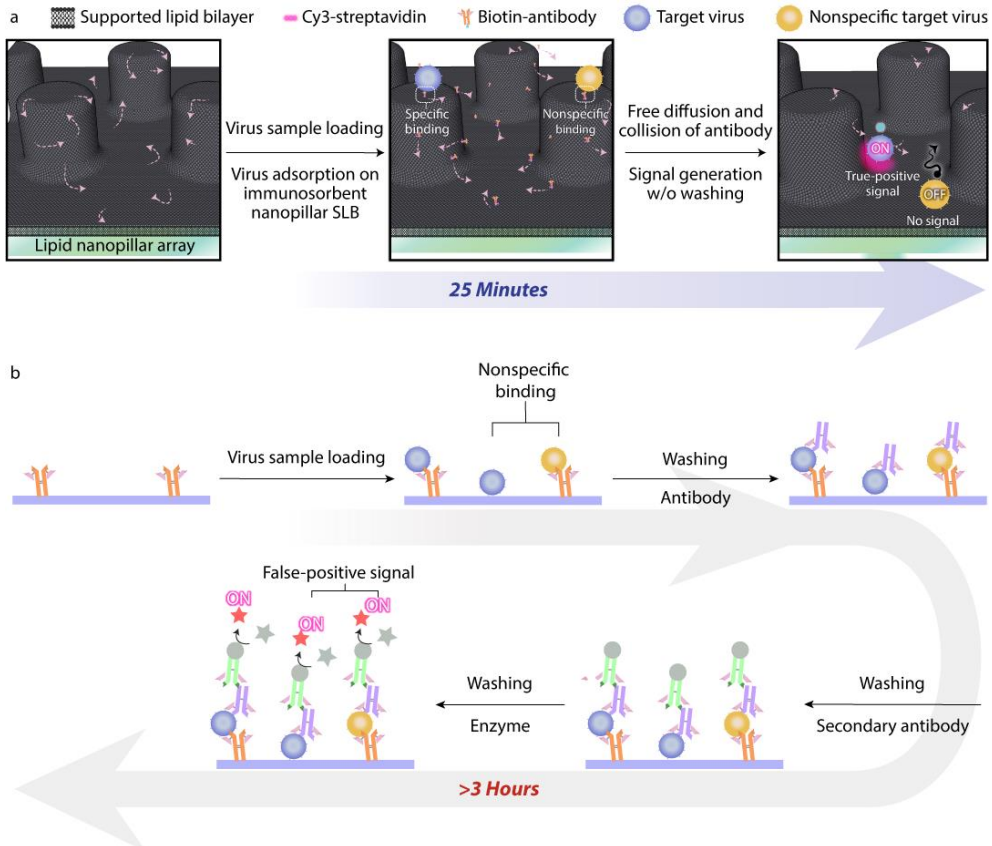

Figure 2-7. Comparison between LNAIA and ELISA. a) LNAIA and b) ELSIA.

2.3. Conclusion

In summary, we developed a new type of immunosorbent assay that can quickly (~25 min) and reliably detect viral targets at very low concentrations (as low as 150 viruses) with an excellent dynamic range (at least 5 orders of magnitude in concentration) based the fluorescent antibody modified LNA with a routinely used fluorescence microscope.

We demonstrated that the engineering of nanopillar structures with

dimensions comparable to the virus could greatly enhance the performance of dynamic and cooperative three-dimensional interactions between viral target and fluid antibody. Lipid bilayer-coated nanopillar substrate can boost the binding kinetics and specificity in virus sensing over the typical physical molecular binding constants of antibodies with conventional assay platforms (e.g., ELISA) (**Figure 2-7**).

Only localized and concentrated fluorescence signals, generated from specific multivalent bindings between virus and antibodies, can be reliably detected with a conventional epifluorescence microscope at an extended exposure time of 300 ms – this can efficiently eliminate false-positive signals by averaging background signal and selectively collect true positive signals.

A multiplexed detection of the target virus in LNAIA using multiple fluorescent channels could resolve many of the difficulties that arise from cross-reactive antibodies in other multiplex immunoassays.[50] We were able to significantly shorten the detection time and minimize assay steps by adopting a 3D-structured labyrinth substrate that maximizes collisions between targets and capture molecules and integrating the transducer and the detector of a biosensor into a single unit and adapting an automated signal analysis. The shortened detection time and minimal assay process on a widely used detection setup can facilitate the use of this assay for the quick, straightforward diagnostic test with

high sensitivity.[51] The LNAIA offers a new detection strategy and platform for fast, sensitive, selective, and reliable detection of viral targets with minimal sampling handling, and could be readily applied in a variety of practical uses, including the development of a rapid response kit for a wide variety of different targets such as proteins and DNA with high sensitivity and a wide dynamic range.

2.4. Experimental section

Preparation of small unilamellar vesicles (SUVs)

In a 50 mL round-bottomed flask, 97.45 mol% 1,2-dioleoyl-sn-glycero-3-phosphocholine (DOPC), 0.05 mol% biotinylated 1,2-dioleoyl-sn-glycero-3-phosphoethanolamine (DOPE), and 2.5 mol% polyethylene glycol (PEG)-DOPE (Molecular Probes, USA) were mixed in chloroform. This lipid solution was evaporated with a rotary evaporator for 1 hr. For the fluorescence recovery after photobleaching (FRAP) experiment to evaluate fluidity of SLB and fluorescence imaging of SLB in the pillar-to-flat boundary area, 1 mol% FITC-DHPE and 1 mol% TexasRed-DHPE were included in the round-bottomed flask, respectively. Using a stream of N_2 gas, the lipid film was completely dried. After being thoroughly dried, the solution was resuspended in DI water (Nanopure water with a minimum resistance >18 MΩ cm^{-1}), transferred to a cryo-tube, and subjected to three freeze-thaw cycles. The final lipid concentration was 4 mg/mL. The solution was extruded 21 times through a polycarbonate (PC) membrane (Whatman, Fisher Scientific) with a pore diameter of 100 nm at 25 ℃. Liposomes of approximately 100 nm were kept at 4 ℃ until use.[11]

Antibody biotinylation

0.2 mg/mL H1N1 antibody (Influenza A H1N1 (A/Puerto Rico/8/1934)

Hemagglutinin, Sinobiological) in 150 mM PBS (50 μL) and 20 μM NHS-biotin (N-hydrocysuccinimidobiotin Thermo Scientific, USA) in DMSO (5 μL) were mixed and incubated for 2 hours at 25 ℃. Non-reacted biotin was removed with desalting columns (Zeba Spin desalting columns 7K MWCO, Thermo Scientific, Rockford, IL, Rockford). The prepared sample described above was loaded in washed desalting columns and 150 mM PBS was added as a stacker. The column was centrifuged at 1500 g for 2 minutes, and the flow-through was retained to modify with streptavidin (STV).

Nanopillar pattern fabrication using spin-on-glass and nanoimprint lithography

A 4-inch glass wafer was cleaned with a plasma asher for 10 min. The glass substrate was spin-coated with IC3-200 spin-on-glass (SOG, Futurrex Inc. USA) at 3000 rpm for 30 sec. The hole-patterned PDMS (SYLGARD 184, Dow Corning, USA) stamp was 200 nm in diameter, 300 nm in-depth, and 400 nm in pitch, and was pressed onto the SOG-coated glass wafer with 2000 kgf cm^{-2} at 150 °C for 10 minutes using ANT-6HO_2 UV/thermal nanoimprint lithography (Korea institute of

machinery and materials, KIMM, Korea). Afterward, the whole stamp was detached from the glass wafer.

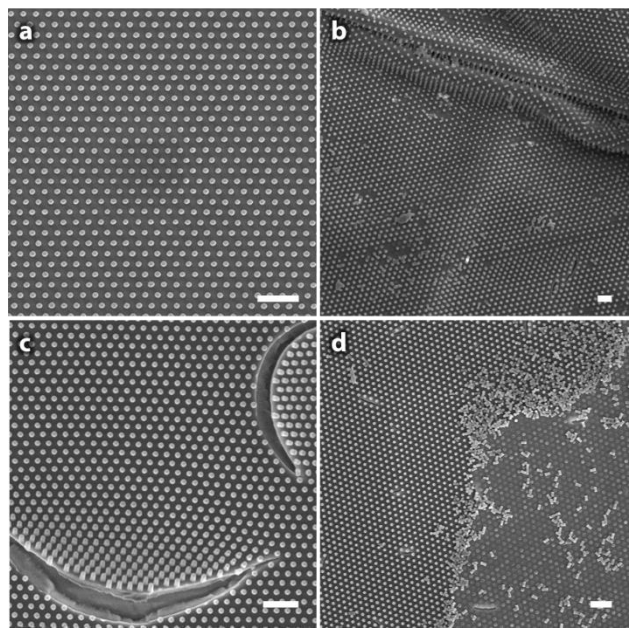

Figure 2-8. Stability of imprinted nanopillar structure depending on methods of giving hydrophilicity and cleaning. Nanopillar arrays are gently cleaned with acetone, then treated with plasma (a), sonicated in acetone for 30 seconds (b), incubated in piranha solution for 30 minutes (c), and incubated in a 1 M NaOH (d). Scale bars are 1μm.

LNAIA kit fabrication.

To fabricate the virus assay kit, a silica nanopillar-patterned substrate was given hydrophilicity and cleaned by plasma asher after washing with ethanol and acetone. On the nanopillar-patterned substrate, a sticker chamber (8 μL) was

attached and previously prepared small unilamellar vesicles were mixed 1:1(v/v) with 150 mM phosphate-buffered saline (PBS) and introduced to the chamber for 30 minutes. After marking a cross line on the bottom of each chamber with a disposable needle and removing excess SUV with 150 mM PBS, 8 μL of 20 μM bovine albumin serum (BSA, Sigma Aldrich) in 150 mM PBS was introduced to inactivate the non-covered area on the nanopillar-patterned substrate. After removing excess BSA with 3 washes with 150 mM PBS, 8 μL of 20 nM Cy3-modified streptavidin (Cy3-STV, Molecular Probes, USA) in 150 mM PBS was introduced for 30 minutes, followed by another wash with 150 mM PBS. Subsequently, biotinylated antibody with an O.D. of 0.02 at 280 nm was introduced for 30 minutes. The chamber was then washed three times with 150 mM PBS before the assay.

LNAIA

A stepwise experimental procedure and LNAIA chamber design are described in **Figure 2-9**. Epifluorescence images of 4 quadrants from each chamber were acquired before and 20 minutes after introducing 8 μL of $1.8 \cdot 10^4$ to $1.8 \cdot 10^9$ viral particles / mL virus (Influenza A/Puerto Rico/8/1934 H1N1 for positive target, and Adenovirus type 5 for negative target) sample with 1 % (v/v) human serum (from human male AB plasma, USA origin, sterile-filtered, Sigma-Aldrich) in PBS to the LNAIA chamber under exposure to a 488 nm laser and 60x lens via TE-2000

(Nikon, Tokyo, Japan). 3 images with an 80×80 μm^2 (512×512 $pixel^2$) field of view and 100 ms exposure time were stacked. The fluorescence images were analyzed to count ΔN (the increased number of fluorescent spots in the four quadrants) using the MOSAIC plugin for Image J software. The four ΔNq (the increased number of fluorescence spots in each quadrant) from a single well were summated as ΔN.

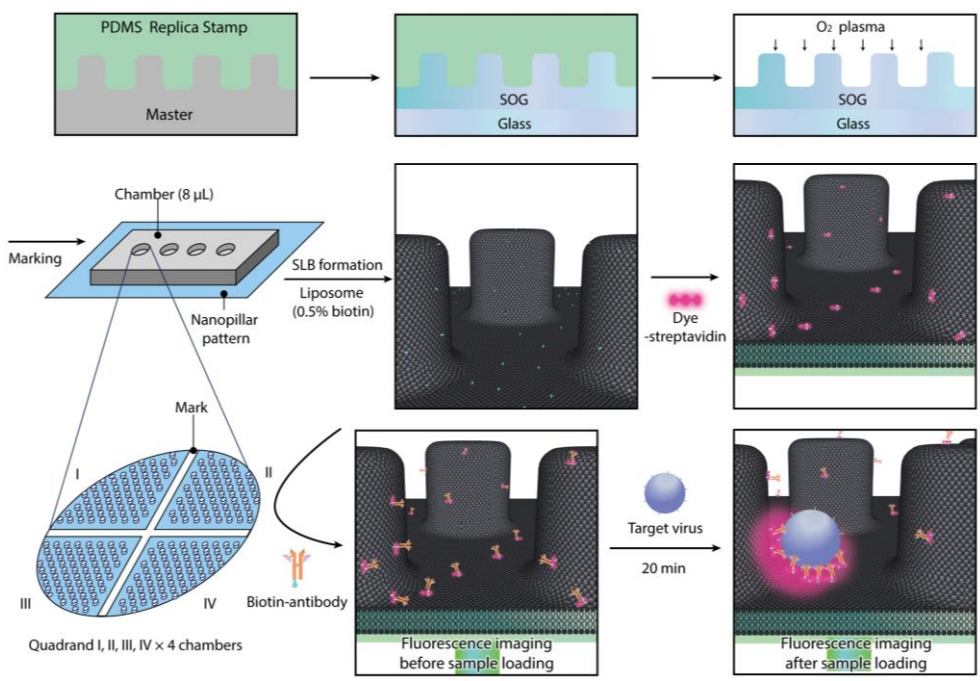

Figure 2-9. A stepwise depiction of the experimental setup.

ELISA

50 μL of $1.8 \cdot 10^4$ to $1.8 \cdot 10^9$ viral particles/mL of virus (Influenza A/Puerto Rico/8/1934 H1N1 for positive target, and Adenovirus type 5 for negative target) samples with 1 % human serum in coating buffer (0.2 M Na_2CO_3/$NaHCO_3$, pH 9.6) were added to individual wells and incubated for 2 hours at room temperature. Wells were washed with 200 μL of PBST (137 mM NaCl, 2.7 mM KCl, 10 mM Na_2HPO_4, 0.1 w/v % Tween 20) 3 times and patted dry on a hand towel. The remaining surface of each well was blocked with 200 μL of 1 % BSA in PBS (137 mM NaCl, 2.7 mM KCl, 10 mM Na_2HPO_4, 1.8 mM KH_2PO_4) for 2 hours at room temperature. Excess BSA was removed with two washes of 200 μL of PBST. 2 μg/mL of primary antibody in PBS with 1% BSA was introduced to each well in a total volume of 100 μL for 2 hours at room temperature. The excess antibody was removed with 4 washes with 200 μL of PBST. 100 μL of secondary antibody with 1 % BSA in PBS was added and incubated for 2 hours at room temperature. Wells were washed 4 times with 200 μL PBST and 50 μL of 3,3',5,5'-Tetramethylbenzidine (TMB) was added. After 15 minutes, each well was treated with 50 μL of 2 M of H_2SO_4 and analyzed by a microplate reader (Multiple Plate Reader, Victor 3, Perkin Elmer, USA).

Side-view of LNA TEM sample preparation

For imaging SLB structure on a nanopillar pattern, the nanopillar labyrinth SLB was fixed in 2% glutaraldehyde and 4% paraformaldehyde in 0.1 M sodium cacodylate buffer (SCB) (pH 7.3) at room temperature for 30 minutes, followed by fixation overnight. The following steps were carried out at 4 ℃ until the graded ethanol series. The sample was washed in 0.1 M SCB with 0.2 M sucrose 3 times and post-fixed with reduced osmium (1% osmium tetroxide with 0.8 % potassium ferricyanide in 0.1 M SCB). After washing with distilled water 3 times, en-bloc staining was carried out with 2 % uranyl acetate. After washing the sample with distilled water 3 times, it was dehydrated with 30 %, 50 %, 70 %, 80 %, and 100 % ethanol in series. Next, the ethanol was exchanged for acetonitrile. Sample infiltration was carried out with a 1:1 mixture of acetonitrile and Spurrs' resin for 2 hours, a 1:2 mixture of acetonitrile and resin for 2 hours, and pure resin overnight at room temperature. The resin was exchanged with fresh resin and baked at 70 ℃ overnight. The bottom silica nanopillar pattern was etched away with 49 % hydrofluoric acid (Sigma Aldrich) in a fume hood, thoroughly washed with distilled water, and dried at 70 ℃ for 30 minutes. The sample was re-embedded with pure resin and baked at 70 ℃ overnight. Subsequently, the resin block was sectioned by ultramicrotome (EM UC7, Leica, Wetzlar, Germany) into 70 nm-thick sections, then collected onto a TEM copper grid (Veco Center Reference Square Grid, 200-mesh, Cu, Tedpella, USA) and post-stained with 2% uranyl

acetate. The prepared grids were imaged with a 120 kV transmission electron microscope (Talos L120C, FEI, Hillsboro, United States).[52]

SEM sample preparation

To determine whether the virus detected by LNAIA was attached between the wall and bottom of the nanopillar labyrinth, the substrate was freeze-dried post-assay, followed by platinum deposition and imaging by SEM (JSM-7800F Prime, JEOL Ltd, Akishima, Japan).

Unit conversion of virus

To obtain the number of the viral particles in the sample of a unit with pfu/mL, a mixture of known concentrations of silica nanoparticles and viral particle samples was imaged via TEM. By measuring the number of viral and silica particles per area in TEM images, we found that there were $7.0 \cdot 10^6$ virus particles in an 8 μL-chamber with $1.0 \cdot 10^7$ pfu/mL.

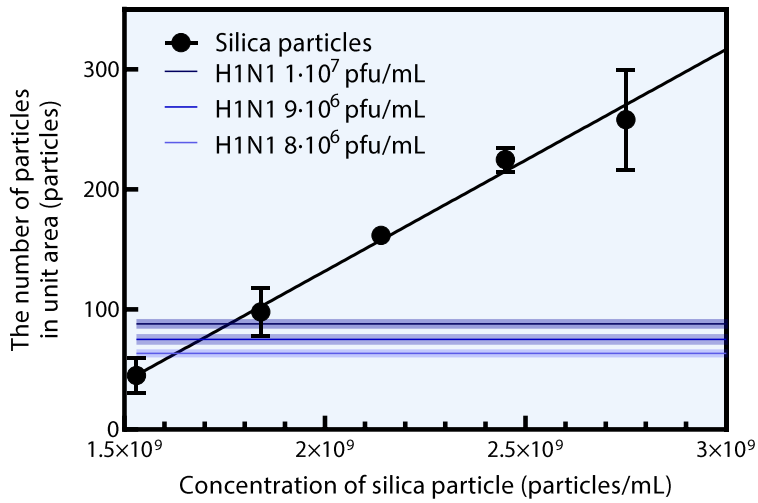

Figure 2-10. Unit conversion of virus into the number of particles/mL using silica nanoparticle. Virus solution with $1.0 \cdot 10^7$ pfu/mL contains $7.0 \cdot 10^6$ virus particles in an 8 μL-chamber.

Reference

1. Castellana, E. T. & Cremer, P. S. Sx`s: From biophysical studies to sensor design. *Surf. Sci. Rep.* **61**, 429–444 (2006).
2. Dziabowska, K., Czaczyk, E. & Nidzworski, D. Detection methods of human and animal influenza virus—current trends. *Biosensors* **8**, 1–24 (2018).
3. Gao, L., Yang, Q., Wu, P. & Li, F. Recent advances in nanomaterial-enhanced enzyme-linked immunosorbent assays. *Analyst* **145**, 4069–4078 (2020).
4. Malik, A. A., Nantasenamat, C. & Piacham, T. Molecularly imprinted polymer for human viral pathogen detection. *Mater. Sci. Eng. C* **77**, 1341–1348 (2017).
5. Tiu, B. D. B. *et al.* Free-Standing, Nanopatterned Janus Membranes of Conducting Polymer-Virus Nanoparticle Arrays. *Langmuir* **32**, 6185–6193 (2016).
6. Surugiu, I., Danielsson, B., Ye, L., Mosbach, K. & Haupt, K. Chemiluminescence imaging ELISA using an imprinted polymer as the recognition element instead of an antibody. *Anal. Chem.* **73**, 487–491 (2001).

7. Jarczewska, M. & Malinowska, E. The application of antibody-aptamer hybrid biosensors in clinical diagnostics and environmental analysis. *Anal. Methods* **12**, 3183–3199 (2020).

8. Harmsen, M. M. & De Haard, H. J. Properties, production, and applications of camelid single-domain antibody fragments. *Appl. Microbiol. Biotechnol.* **77**, 13–22 (2007).

9. De Meyer, T., Muyldermans, S. & Depicker, A. Nanobody-based products as research and diagnostic tools. *Trends Biotechnol.* **32**, 263–270 (2014).

10. Akama, K., Shirai, K. & Suzuki, S. Droplet-Free Digital Enzyme-Linked Immunosorbent Assay Based on a Tyramide Signal Amplification System. *Anal. Chem.* **88**, 7123–7129 (2016).

11. Farka, Z. *et al.* Advances in Optical Single-Molecule Detection: En Route to Supersensitive Bioaffinity Assays. *Angewandte Chemie - International Edition* vol. 59 10746–10773 (2020).

12. Sensing, F. *et al.* Restriction of receptor movement alters cellular response: Physical force sensing by EphA2. *Science (80-.).* **327**, 1380–1385 (2010).

13. Ma, V. P. Y. *et al.* Ratiometric tension probes for mapping receptor forces and clustering at intermembrane junctions. *Nano Lett.* **16**, 4552–4559 (2016).

14. Hartman, K. L., Kim, S., Kim, K. & Nam, J. M. Supported lipid bilayers as dynamic platforms for tethered particles. *Nanoscale* **7**, 66–76 (2015).

15. Lee, Y. K., Lee, H. & Nam, J. M. Lipid-nanostructure hybrids and their applications in nanobiotechnology. *NPG Asia Mater.* **5**, e48-13 (2013).

16. G. Duff, D., Baiker, A. & P. Edwards, P. A new hydrosol of gold clusters. 1. Formation and particle size variation. *Langmuir* **9**, 2301–2309 (2002).

17. Yang, T., Jung, S. Y., Mao, H. & Cremer, P. S. Fabrication of phospholipid bilayer-coated microchannels for on-chip immunoassays. *Anal. Chem.* **73**, 165–169 (2001).

18. Kim, S. S. *et al.* Nanotherapeutics for Gene Modulation that Prevents Apoptosis in the Brain and Fatal Neuroinflammation. *Mol. Ther.* **26**, 84–94 (2018).

19. Pardi, N., Hogan, M. J., Porter, F. W. & Weissman, D. mRNA vaccines-a new era in vaccinology HHS Public Access. *Nat Rev Drug Discov* **17**, 261–279 (2018).

20. Ono, A. & Freed, E. O. Plasma membrane rafts play a critical role in HIV-1 assembly and release. *Proc. Natl. Acad. Sci.* **98**, 13925–13930 (2001).

21. Qi, S. Y., Groves, J. T. & Chakraborty, A. K. Synaptic pattern formation during cellular recognition. *Proc. Natl. Acad. Sci.* **98**, 6548–6553 (2001).

22. Kam, L. C. Capturing the nanoscale complexity of cellular membranes in supported lipid bilayers. *J. Struct. Biol.* **168**, 3–10 (2009).

23. Lee, Y. K., Kim, S., Oh, J. W. & Nam, J. M. Massively parallel and highly quantitative single-particle analysis on interactions between nanoparticles on supported lipid bilayer. *J. Am. Chem. Soc.* **136**, 4081–4088 (2014).

24. Seo, J., Kim, S., Park, H. H., Choi, D. Y. & Nam, J. M. Nano-bio-computing lipid nanotablet. *Sci. Adv.* **5**, 1–14 (2019).

25. Kim, S. *et al.* Optokinetically Encoded Nanoprobe-Based Multiplexing Strategy for MicroRNA Profiling. *J. Am. Chem. Soc.* **139**, 3558–3566 (2017).

26. Groves, J. T., Ulman, N. & Boxer, S. G. Micropatterning fluid lipid bilayers on solid supports. *Science (80-.).* **275**, 651–653 (1997).

27. Groves, J. T., Mahal, L. K. & Bertozzi, C. R. Control of cell adhesion and growth with micropatterned supported lipid membranes. *Langmuir* **17**, 5129–5133 (2001).

28. Motegi, T. *et al.* Effective brownian ratchet separation by a combination of molecular filtering and a self-spreading lipid bilayer system. *Langmuir* **30**, 7496–7501 (2014).

29. Tsai, J., Sun, E., Gao, Y., Hone, J. C. & Kam, L. C. Non-Brownian diffusion of membrane molecules in nanopatterned supported lipid bilayers. *Nano Lett.* **8**, 425–430 (2008).

30. Werner, J. H. *et al.* Formation and Characterization of Supported Phospholipid Membranes on a Periodic Nanotextured Substrate. 87131 (2009).

31. Schmitt, E. K., Vrouenraets, M. & Steinem, C. Channel activity of OmpF monitored in nano-BLMs. *Biophys. J.* **91**, 2163–2171 (2006).

32. Favero, G. *et al.* Glutamate receptor incorporated in a mixed hybrid bilayer lipid membrane array, as a sensing element of a biosensor working under flowing conditions. *J. Am. Chem. Soc.* **127**, 8103–8111 (2005).

33. Römer, W. *et al.* Channel activity of a viral transmembrane peptide in micro-BLMs: Vpu 1-32 from HIV-1. *J. Am. Chem. Soc.* **126**, 16267–16274 (2004).

34. Simon, A. *et al.* Formation and stability of a suspended biomimetic lipid bilayer on silicon submicrometer-sized pores. *J. Colloid Interface Sci.* **308**, 337–343 (2007).

35. Mey, I. *et al.* Local membrane mechanics of pore-spanning bilayers. *J. Am. Chem. Soc.* **131**, 7031–7039 (2009).

36. Lou, H. Y. *et al.* Dual-functional lipid coating for the nanopillar-based capture of circulating tumor cells with high purity and efficiency. *Langmuir* **33**, 1097–1104 (2017).

37. Wu, H. J. *et al.* Membrane-protein binding measured with solution-phase plasmonic nanocube sensors. *Nat. Methods* **9**, 1189–1191 (2012).

38. Lee, Y. K. & Nam, J. M. Electrofluidic lipid membrane biosensor. *Small* **8**, 832–837 (2012).

39. Di Iorio, D., Verheijden, M. L., Van Der Vries, E., Jonkheijm, P. & Huskens, J. Weak Multivalent Binding of Influenza Hemagglutinin Nanoparticles at a Sialoglycan-Functionalized Supported Lipid Bilayer. *ACS Nano* **13**, 3413–3423 (2019).

40. Vemula, S. V. *et al.* Current Approaches for Diagnosis of Influenza Virus Infections in Humans. *Viruses* **8**, 1–15 (2016).

41. Saylan, Y., Erdem, Ö., Ünal, S. & Denizli, A. An alternative medical diagnosis method: Biosensors for virus detection. *Biosensors* **9**, 65 (2019).

42. Chen, Y. *et al.* One-step detection of pathogens and viruses: Combining magnetic relaxation switching and magnetic separation. *ACS Nano* **9**, 3184–3191 (2015).

43. Groves, J. T. & Dustin, M. L. Supported planar bilayers in studies on immune cell adhesion and communication.Title. *J. Immunol. Methods* **278**, 19–32 (2003).

44. Jonsson, M. P., Jönsson, P., Dahlin, A. B. & Höök, F. Supported lipid bilayer formation and lipid-membrane-mediated biorecognition reactions studied with a new nanoplasmonic sensor template. *Nano Lett.* **7**, 3462–3468 (2007).

45. Van Weerd, J. *et al.* On-chip electrophoresis in supported lipid bilayer membranes achieved using low potentials. *J. Am. Chem. Soc.* **136**, 100–103 (2014).

46. Kim, S. *et al.* Plasmonic Nanoparticle-Interfaced Lipid Bilayer Membranes. *Acc. Chem. Res.* **52**, 2793–2805 (2019).

47. Nigel J. Dimmock, Andrew J. Easton, K. N. L. *Introduction to Modern Virology*. (Wiley-Blackwell, 2016).

48. David M. Knipe, P. H. *Fields Virology*. (Lippincott Williams & Wilkins, 2013).

49. Mitnaul, L. J. *et al.* Balanced Hemagglutinin and Neuraminidase Activities Are Critical for Efficient Replication of Influenza A Virus. *J. Virol.* **74**, 6015–6020 (2000).

50. Juncker, D., Bergeron, S., Laforte, V. & Li, H. Cross-reactivity in antibody microarrays and multiplexed sandwich assays: Shedding light on the dark side of multiplexing. *Curr. Opin. Chem. Biol.* **18**, 29–37 (2014).

51. Yang, F. *et al.* A bubble-mediated intelligent microscale electrochemical device for single-step quantitative bioassays. *Adv. Mater.* **26**, 4671–4676 (2014).

52. Hanson, L., Lin, Z. C., Xie, C., Cui, Y. & Cui, B. Characterization of the cell-nanopillar interface by transmission electron microscopy. *Nano Lett.* **12**, 5815–5820 (2012).

국문 초록

바이러스성 전염병은 인류의 건강을 위협할 뿐만 아니라 전세계적인 경제적인 타격도 유발한다. 이에 따라 신속하고 민감하며 표적-선택적인 바이러스 검지 기술이 요구된다. 효소면역 흡착법 (Enzyme-linked immunosorbent assay) 는 주로 평평한 기판 위에서 이루어지는데 바이러스 자체를 후 처리 할 필요없이 검지할 수 있어서 널리 이용되어왔으나 민감도가 낮고, 정량 범위가 좁으며, 사용하는 항체에 따라 선택성도 낮아진다. 또한 단계적으로 여러 시료를 도입하고 세척하는 과정에서 시간과 노동력이 많이 필요하다.

본 연구에서는 신속하고 민감하게 표적 바이러스만을 선택적으로 검지할 수 있는 지질 나노필라 어레이기반 면역흡착 어세이 (Liquid-nanopillar-array-based immunosorbent assay, LNAIA) 법을 개발하였다. 3 차원 구조를 갖는 나노필라 어레이 상에 지질 지중층을 이용하여 유동적으로 움직일 수 있는 형광-항체를 도입하고, 표적 바이러스와 결합시켜 형성되는 형광신호를 측정하였다. 나노필라 형태의 지질 이중층과 바이러스간의 다중결합이 항체를 통해 형성되면 광학 분해능보다 좁은 영역에 형광이 밀집되면서 보편적인 형광 현미경으로도 단일 개체 단위로 바이러스를 검지 할 수 있다. 형광 이미지를 자동화된 소프트웨어를 이용하여 분석하여 바이러스 시료를 도입한 후 25 분 이내에 2 차 항체나

효소등의 시료를 추가적으로 도입하지 않고도 최소 150 개의 H1N1 Influenza A 바이러스를 검지 할 수 있었다.

키워드 : 바이오센서, 면역흡착 어세이, 지질 나노필라 어레이, 지지형 지질 이중층, 바이러스 검지

학번 : 2014-21220